Optimizing an Event-Driven Detector for High Speed Scanning Diffraction Measurements in the Transmission Electron Microscope

Rohini Ghosh[1,2], Steve E. Zeltmann[2,3], and David A. Muller[3]

[1]*Department of Chemical and Environmental Engineering, University of Arizona, Tucson, AZ*
[2]*PARADIM, Department of Materials Science and Engineering, Cornell University, Ithaca, NY*
[3]*School of Applied and Engineering Physics, Cornell University, Ithaca, NY*

Abstract

Modern pixel array detectors used in advanced imaging techniques such as ptychography typically record diffraction data by integrating signals over fixed exposure times. In contrast, event-driven detectors such as the Timepix4 enable faster data acquisition by continuously registering the time of arrival and position of individual events. However, this advantage comes with challenges such as increased susceptibility to saturation. In this study, we use Monte Carlo simulations to evaluate the performance of a back-thinned sensor layer and pulse-counting strategy in an event-driven Timpeix4 detector. Our results demonstrate sensor thinning combined with optimized thresholding reduces lateral charge spread and limits the number of counts generated per incident electron, all with minimal tradeoff in the detector's DQE.

Introduction

The development of direct electron detectors has been instrumental in the field of electron microscopy. Earlier systems relied on scintillator-coupled detectors, in which the electron beam was first converted into photons, which were then detected. This two-step process of electron-to-photon conversion and subsequent photon transport significantly reduced the detector's detective quantum efficiency (DQE), prompting the need for a more efficient solution[1]. Direct electron detectors address this limitation by being directly exposed to the electron beam, eliminating inefficiencies inherent to scintillator-based systems.

Hybrid pixel array detectors, a widely used class of direct electron detectors, comprise a pixelated silicon sensor layer bonded to an integrated circuit via solder bump bonds. Incident electrons are absorbed in the reverse-biased sensor layer, generating electron-hole pairs that are collected and transferred to the application-specific integrated circuit (ASIC). To ensure full energy deposition from high-energy electrons, the sensor layer is typically thick, allowing for high lateral charge spread and necessitating larger pixel pitches, such as the 150 µm pitch used in the EMPAD-G2. These detectors operate in charge integration mode, where the pixel output is proportional to the total collected charge [2].

Conventional pixel array detectors operate using a frame-based readout mechanism, recording the signal in each pixel after a defined exposure period. In contrast, event-driven detectors enable faster acquisition and real-time data processing by continuously recording individual electron events as they occur. The Timepix4, the latest generation of Medipix readout ASICs, features a 448 × 512 pixel array with a 55 µm pitch and supports event rates of ~3.6 MHz/mm²/s [3]. When operated in data-driven mode, Timepix4 outputs the pixel coordinates of each hit, along with the time of arrival and the time over threshold of the event.

Event-driven detectors such as the Timepix4 face a further limitation with pixel saturation; following pixel activation, any subsequent incident electrons will not be registered during the data processing period, forcing an upper limit on the dose which can be processed[4]. For this reason, event-driven STEM has typically been limited to low-dose applications.

One strategy to mitigate pixel saturation is back-thinning of the silicon sensor layer, thereby reducing lateral spread of charge and lowering the counts generated per incident electron. However, thinning allows electrons to transmit through the sensor, leading to variable energy deposition characterized by a Landau distribution. This variability renders traditional charge integration ineffective. Therefore, a pulse-counting approach must be adopted, in which the energy deposited in each pixel is compared against a programmable threshold to register discrete events. However, pulse-counting introduces digitization errors in the recorded counts, as threshold adjustments lead to

tradeoffs between multiple adjacent pixels being triggered by a single electron and electrons failing to be counted altogether.

This paper evaluates the viability of a detector implementing a back-thinned sensor layer and a pulse-counting strategy in event-driven detectors. Monte Carlo simulations were employed to model electron trajectories and lateral charge spread of 300 keV electrons through silicon sensor layers of varying thickness. The resulting impacts on the DQE and modulation transfer function (MTF) are analyzed to assess overall detector performance.

Methods

Monte Carlo simulations were performed using the CASINO software to model 300 keV electrons incident normal to a bulk silicon sensor layer. CASINO simulates electron trajectories as a series of discrete elastic scattering events, governed by the screened Rutherford cross section. Inelastic interactions are approximated as continuous energy loss along the electron's path [5]. This approach enables characterization of the energy deposition profile resulting from individual electron events.

To simulate pulse-counting behavior, the lateral energy deposition profile from each incident electron was mapped onto the 55 μm pixel grid of the Timepix4. A count was registered in any pixel where the deposited energy exceeded a defined threshold. To mimic uniform illumination and eliminate artifacts from variable entry positions, electron entry coordinates were randomized within each pixel when calculating mean counts and DQE. Sensor thinning was modeled through termination of electron trajectories at specified depths within the silicon layer.

The DQE is defined as the ratio of the output signal-to-noise ratio (SNR) to the input SNR, quantifying how effectively a detector preserves signal quality relative to statistical noise. When individual electron events can be resolved, the zero-frequency DQE, DQE(0), can be calculated from the probability distribution of recorded counts using the ratio of the squared first moment to the second moment of the distribution[6].

The modulation transfer function (MTF) quantifies the ability of a detector to preserve image contrast as a function of spatial frequency, reflecting how well spatial details are transferred from object to image. The MTF can be calculated by taking the Fourier Transform of the 1D point spread function (PSF) of a point source and multiplying by the response of a perfect detector, $sinc(\frac{\pi\omega}{2})$ [7].

Results and Discussion

The vertical cross-section of the energy distribution (Figure 1) demonstrates a characteristic "teardrop" profile of energy deposition for a simulation of 100,000 electrons at 300 keV beam energy. At the beam location, there is an initial area of high deposition and a balloon-like spread of energy outwards and downwards, quickly exceeding the 55 μm pitch of the Timepix4.

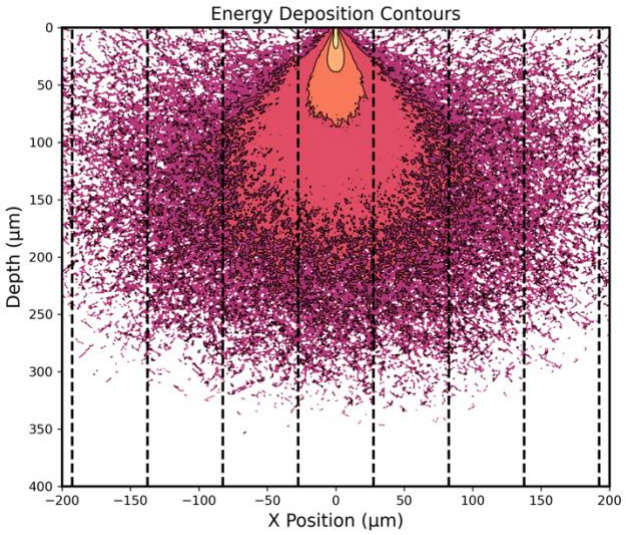

Figure 1. Vertical cross section of the energy deposition of 300 keV electrons in 500 μm silicon from a Monte Carlo simulation of 100,000 electrons.

Figures 2a–2c present the mean counts per electron, DQE(0), and MTF at Nyquist frequency for sensor thicknesses ranging from 50 to 500 μm and threshold values between 5 and 140 keV. Increasing the threshold reduces the number of recorded counts per electron, with very high thresholds resulting in mean counts close to zero where a significant fraction of electrons are undetected. As hypothesized, thinning of the sensor layer allows the charge spread to be terminated before maximum lateral spread has been achieved, resulting in lower mean counts for thin sensors at a given threshold. This mitigates pixel saturation, as fewer pixels activated per electron reduces the likelihood of overlapping events and allows more accurate processing at higher electron flux (Figure 2a).

An increase in the threshold leads to a rapid decline in DQE(0), driven by a greater number of electrons left uncounted. Similarly, as the sensor is thinned, more electrons transmit through without depositing sufficient energy to be counted, reducing DQE(0). Further, thinner sensors exhibit increased variability in the energy deposited per electron, leading to an increase in the variance compared to mean in the

number of counts generated per electron, thus degrading DQE.

An exception is observed for the 50 µm sensor at 10 keV and 20 keV thresholds, which shows improved DQE compared to the 100 µm sensor at the same thresholds, likely due to reduced energy deposition variance in the thinner layer (Figure 2b). This suggests that at low thresholds, very thin sensors may provide more consistent pulse-counting behavior under specific energy deposition regimes.

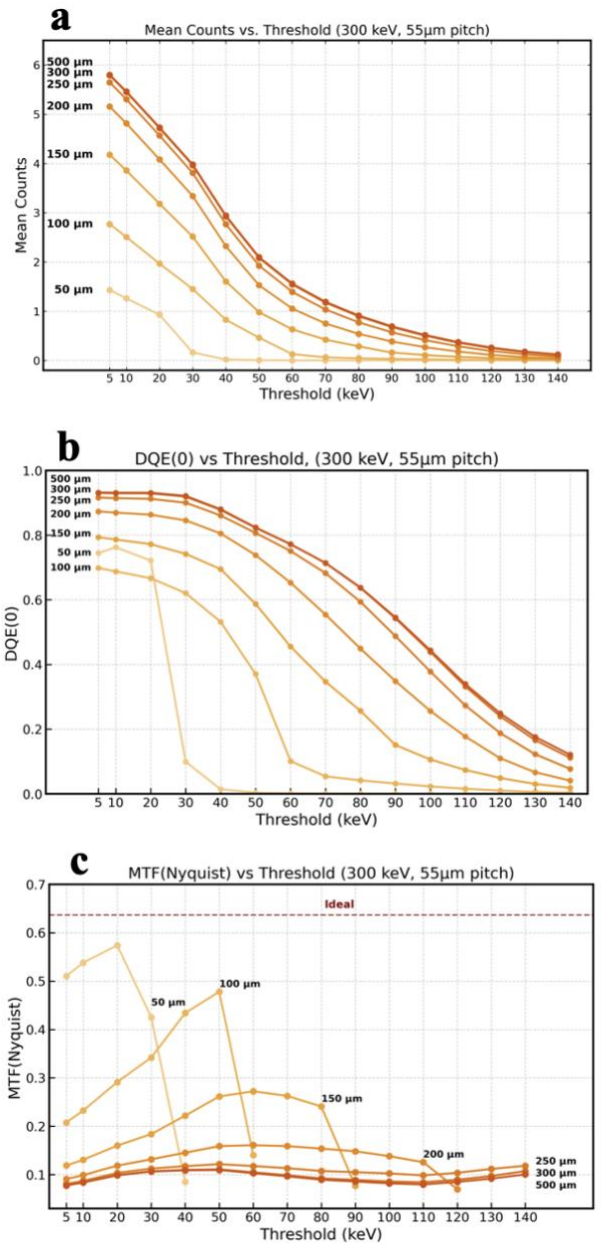

Figure 2. Description of detector characterization parameters as a function of threshold for various sensor layer thicknesses: (a) mean counts per electron, (b) DQE(0), and (c) MTF(Nyquist).

Sensor-layer thinning significantly reduces the spread of pixel activations, with the MTF at Nyquist frequency approaching that of an ideal detector for certain combinations of sensor thickness and threshold. In thinned sensors, the MTF initially improves with increasing threshold, as higher thresholds suppress low-energy peripheral charge, resulting in a more sharply peaked point spread function (PSF). However, above a certain threshold, the MTF drops sharply as the mean count per electron approaches zero. In contrast, thick sensors exhibit little to no dependence of MTF on threshold. This suggests that the lateral energy spread in thick sensors is sufficiently large compared to the pixel size that thresholding has minimal effect on sharpening the PSF profile (Figure 2c).

These results highlight a fundamental tradeoff between MTF and DQE. As the sensor is thinned, the MTF improves due to reduced lateral energy spread, resulting in a sharper PSF; however, the DQE degrades due to increased variability in the counts generated per electron. The threshold can be lowered to improve the DQE, although this would broaden the PSF from the inclusion of more peripheral counts, impacting the MTF. Among the tested configurations, the 50 µm sensor with a 10 keV and 20 keV threshold offers a favorable compromise, providing a reasonable balance between DQE and MTF, along with a low mean count per electron that reduces pixel saturation.

Both the mean counts per electron and the DQE(0) provide insight into the maximum speed, and by extension the maximum electron dose, at which a detector can operate. A higher mean count per electron corresponds to a lower allowable electron dose, while lower DQE requires a greater electron dose to maintain image quality. A detector with both parameters equal to unity represents the theoretical optimum for detector performance, allowing for maximum operational speed or maximum electron dose.

Figure 3a displays the mean counts per electron as a function of inverse DQE. As discussed previously, the thinned sensors showed degraded DQE due to increased variability in the counts generated. Thinned sensors show lower DQE(0) for the same achieved mean counts value compared to thick sensors. The 50 µm sensor is an exception to this trend, showing improved DQE values compared to thick sensors for the same mean counts per electron of around one.

Multiplication of mean counts per electron by the inverse DQE yields a useful performance parameter, where lower values indicate performance closer to the theoretical optimum. This parameter also enables comparison of the relative magnitude of changes in mean counts and DQE across different detector configurations. Figure 3b plots this product as a

function of threshold for various sensor thicknesses. For a given threshold, sensor thinning results in a marked reduction in this parameter, indicating the reduction in mean counts greatly exceeds the extent of DQE degradation.

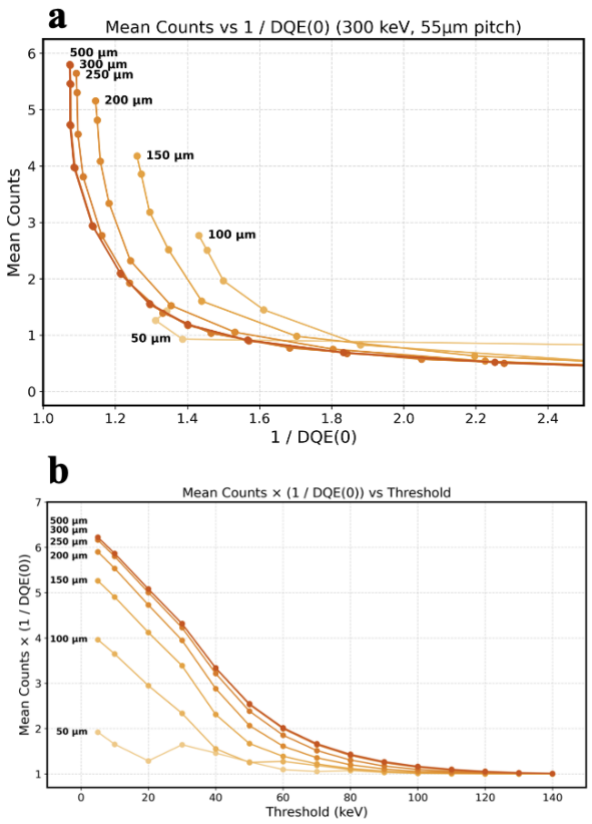

Figure 3. Comparison in the values of DQE(0) and mean counts for each threshold and thickness combination. (a) Plot of mean counts versus inverse DQE for each thickness. Points of increasing inverse DQE within each thickness correspond to increasing threshold. (b) Plot of mean counts multiplied by inverse DQE as a function of threshold for different sensor layer thicknesses.

As the threshold is increased, the interpretability of this parameter decreases. At sufficiently high thresholds, an incident electron may only deposit enough energy to activate a single pixel. In this regime, using the definition of DQE(0) as the ratio of the squared mean to the variance of the counts-per-electron distribution, the DQE(0) will converge towards the value for mean counts per electron. At these high thresholds, the value for both DQE and mean counts fall significantly below the ideal value of unity; for instance, at a threshold of 80 keV, the mean counts per electron drops below 0.75 for all sensor thicknesses.

Within the threshold range where this metric retains physical meaning, the thinned 50 µm sensor at 10 and 20 keV thresholds demonstrates superior performance, with a product of the mean counts and inverse DQE lower than that of the thicker detectors.

Conclusion

Monte Carlo simulations were employed to assess the effects of sensor-layer thinning and thresholding on the performance of a pixel array detector, with the goal of reducing counts per electron to mitigate pixel saturation in event-driven systems. The results revealed a tradeoff between detective quantum efficiency (DQE) and modulation transfer function (MTF): while thinning the sensor layer reduced lateral charge spread and improved MTF, it also led to a decline in DQE due to increased variability in charge deposition. However, by combining sensor thinning with an appropriately low threshold, the degradation in DQE can be limited. Further, the ratio between mean counts and DQE(0) was considered to assess optimal detector operation speed, with 50 µm sensor at low thresholds showing an improvement over the thick sensors. Future work should focus on experimental validation of these findings through direct characterization of the physical detector.

Acknowledgements

I would like to thank my mentor Steve Zeltmann and principal investigator David Muller for their support and guidance in this project. This work was funded by the Platform for the Accelerated Realization, Analysis, and Discovery of Interface Materials (PARADIM) and the National Science Foundation (NSF).

References

[1] B. D. A. Levin, *J. Phys. Mater.*, **4**, (2021), 042005.
[2] H. T. Philipp et al., *Microsc. Microanal.* **28**, (2022), 425–440.
[3] Llopart et al., *JINST.* **17**, (2022), C01044.
[4] Annys et al., *Ultramicroscopy*. **227**, (2025), 114206.
[5] Demers et al., *Scanning*. **33**, (2011), 135-146
[6] McMullan et al., *Ultramicroscopy*. **109**, (2009), 1126-1143.
[7] Ruskin et al., *J. Struct Biol*. **184**, (2013), 385-393